Journal of Engineering and Technology for Industrial Applications

ITEGAM-JETIA

Manaus, v10. n.50, p. 01-09. November./ December., 2024.
DOI: https://doi.org/10.5935/jetia.v10i50.1144

ISSN ONLINE: 2447-0228

RESEARCH ARTICLE OPEN ACCESS

MECHANICAL PROPERTIES CHARACTERIZATION OF WELDED 3CR12 STAINLESS STEEL

Thabo Nelson Mathonsi

University of Johannesburg, Faculty of Engineering, Johannesburg, South Africa

https://orcid.org/0000-0003-4801-685

Email: tmathonsi@uj.ac.za

ARTICLE INFO

Article History
Received: June 5, 2023
Revised: July 1, 2023
Accepted: August 10, 2024
Published: November 30, 2024

Keywords:
3CR12 Stainless Steel,
Welding,
Mechanical Properties
Microstructure,
Heat-affect-zone (HAZ)

ABSTRACT

The use of metal inert gas (MIG) welding for joining metals frequently results in the change of the mechanical properties and the microstructure of the metal at the welded areas. This is due to the welding heat input and heat transfer. 3CR12 is a low-cost special stainless steel containing 12% chromium. It is considered to have good mechanical properties and corrosion resistance as a base metal, and understanding how these properties change as a result of MIG welding enables the drawing of proper conclusions regarding the properties of MIG welded 3CR12 stainless steel. However, little is known about its properties and behavior after welding with metal inert gas (MIG) welding, which is the most common welding process for welding stainless steel, and little is known about its weldability. Due to inadequate information about MIG welded 3CR12 stainless steel, it is hard to make a reliable statement about its properties and behavior. Thus, necessitating the need to gain knowledge regarding MIG welded 3CR12 stainless steel. This paper aims to characterize the mechanical properties of welded 3CR12 stainless steel. The focus is on investigating how the mechanical properties and the microstructure of 3CR12 stainless steel evolve due to MIG welding.

I. INTRODUCTION

It must define the problem and importance of the research carried out, it presents a (not very extensive) review of the literature on the subject of the article, including the authors' contributions to the state of the art. If you use abbreviations or acronyms, first write the words that identify them and then, in parentheses, the acronym. This set also establishes the research question, the objectives of the work and hypothesis, if necessary, the importance and limitations of the study. Establishes the method used at work. It is written in the present tense. Industrial equipment and pipes can be made from a variety of metallic materials. However, carbon steel still has the greatest applicability in the construction of the majority of equipment [1]. Although carbon steels can be utilized in a wide range of applications, they do have some technical limits, particularly in low-temperature and corrosive conditions. This is why they are regarded as general-purpose materials. While carbon steels lack some characteristics, alloy and stainless steels do, but in comparison to carbon steel, they have substantially greater production costs as well as expenditures associated with welding and assembly for industrial installations [2].

Despite their lower cost, carbon steels are not resistant to corrosion or erosion condition which generates undesirable contaminant residues. For this reason, carbon steel cannot be used directly in situations where it can contaminate the final product. In these situations, carbon steel is coated with more durable metallic or non-metallic compounds or other alloys to provide protection at a lower cost. Stainless steels are an example of this that are easily weldable [3]. Austenitic stainless steels are used specifically for building and protecting equipment and pipelines made of carbon steel from corrosion. With the exception of some ferritic steels with a chromium content of up to 17%, which have acceptable weldability and an expansion coefficient that is comparable to that of carbon steel, it is not advised to use many types of stainless steel, such as ferritic and martensitic, as structural steel or welded steel [4].

Middleburg Steel and Alloy (Pty) Ltd (later known as Columbus Stainless Steel) developed 3CR12 from AISI 409 stainless steel in 1970 [5]. 3CR12 is a low carbon utility ferritic stainless steel that complies with ASTM A240 and EN 1008-2 requirements. The single ferrite phase that exists in AISI 409 at high temperatures causes substantial grain growth in the material, which is bad for toughness, ductility, and the ductile to brittle

transition temperature (DBTT) [6], [7]. This prompted the creation of 3CR12, a corrosion-resistant steel that would successfully replace coated carbon steel in typical corrosive situations and be reasonably inexpensive compared to other stainless steels like austenitic stainless steel [8].

To create dual phase structure (ferrite and austenite) at high temperatures, where one phase inhibits the formation of the other's grain, 3CR12 was produced by carefully balancing ferrite and austenite stabilizers [9]. Subsequently it has been found that 3CR12 has a grain structure that is considerably finer than that of AISI 409, which improves its weldability and mechanical qualities [7]. So far, it's important to note that 3CR12 also experiences grain growth. The manufacturer asserts that 3CR12 maintains its toughness to this extent when welded to thicknesses of up to 30 mm without post welding heat treatment (PWHT) [10].

There are two variants of 3CR12 i.e., un-stabilized (3CR12L) and titanium (Ti) stabilized grade (3CR12Ti) with their chemical compositions presented in Table 1.

Table 1: Composition of unsterilized (3CR12Ti) and titanium stabilized (3CR12L).

Grade	3CR12Ti	3Cr12L
C	0.03	0.03
Si	1	1
Mn	2	1.2
P	0.04	0.04
S	0.03	0.015
N	-	0.03
Cr	10.5-12.5	0.3-1
Ni	1.5	-
Other	Ti:4(C+N)0.6	-

Source: [10].

3CR12 is an intriguing and less expensive option to austenitic stainless steels (304, 316L) is 3CR12 [11]. Currently, some companies in South Africa i.e., Transnet Freight Rail, and Anglo Gold use 3CR12 in mine train wagons, due to its excellent corrosion resistance [12]. Nevertheless, little information specifically dedicated to the understanding mechanical properties behavior when welding 3CR12 stainless steel is available in the literature whereas austenitic grades are much more covered [13], [14], [15], [16] The most common research outputs in relation to stainless steel 3CR12 is based on determining the optimum welding material [17], [18].

This paper aims to characterize the mechanical properties of welded 3CR12 stainless steel. The focus is on investigating how the mechanical properties and the microstructure of 3CR12 stainless steel evolve due to MIG welding.

II. EXPERIMETAL PROGRAM

II.1 MATERIAL

The base material used was 3CR12 stainless steel supplied by Macsteel as 100 ×100 × 3 mm off-cut plate (see Figure 1) Table 2-1 shows mechanical properties of the base metal (obtained from the manufacturer's catalogue). Several researchers [18], [19] found that 308L welding material is the most suitable material for welding 3CR12 stainless steel. Chemical composition of the 308L weld wire was obtained from the manufacturer's catalogue [20].

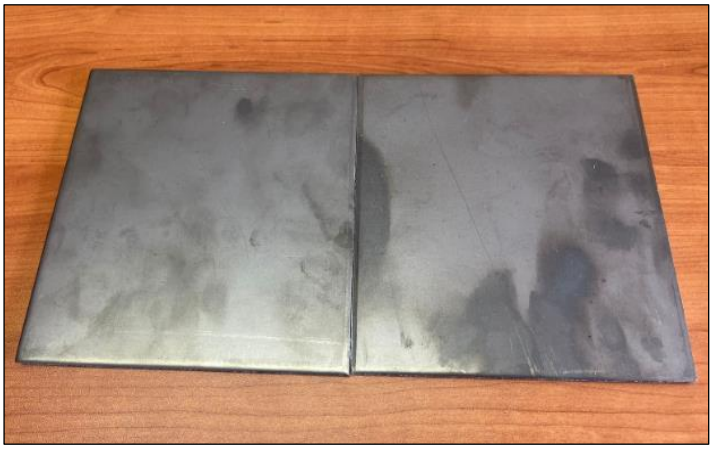

Figure 1: 3CR12 stainless steel.
Source: Authors, (2024).

Table 2: Mechanical properties of 3CR12 stainless steel material.

Material	Tensile Strength (MPa)	Yield Strength (MPa)	%Elongation	Hardness (H)
3CR12	460	300-450	18	173

Source: [10].

III. WELDING PROCEDURE

Welding was conducted at Roan Engineering (Pty LTD) in Johannesburg, South Africa. The welding process was carried out using a six-axis MOTOMAN AR1440 arc welding robot (see Figure 2) with rated output current and voltage of 30-350A and 12-36V respectively.

Figure 2: Yaskawa robotic welder.
Source: [21].

The welder was configured to reverse polarity with welding grade argon shielding gas at 15 l/min flow rate. Welding was carried out (in accordance with the manufacturer's recommendation) as shown in Table 3.

Table 3: Welding procedure.

Welding Process	MIG
Filler Metal	308L (1.6 mm)
Tip to work distance	15 mm
Wire Feed Tare	6 m/min

Source: Authors, (2024).

III.1 WELDING PARAMETERS

According to [18], [19], [22] the optimum heat input (HI) input range for welding 3CR12 stainless steel is between 0.5 – 1.5 kJ/mm. To fully understand the mechanical behavior of 3CR12 stainless steel when welded, a variety of HI values (within and outside the optimum range) were selected. Since heat input is a function of the welding voltage, current, and speed. Based on the range of voltage, current, and welding speed used in welding 3CR12 stainless steel from the literature, the values resulting in the required HI values were selected. The mechanical properties were investigated at the parameters and the resulting heat input, as shown in Table 4.

Table 4: Welding parameters and resulting heat inputs.

Sample No.	Voltage (V)	Current (A)	Welding Speed (mm/s)	Heat Input (kJ/mm)
1	180	11.5	4.5	0.35
2	190	12.5	4.0	0.45
3	230	17.0	3.0	1
4	260	21.0	2.5	1.64
5	270	22.0	2.5	1.75

Source: Authors, (2024).

IV. SAMPLE PREPARATION

IV.1 MATERIAL MICROSTRUCTURE AND MICROHARDNESS

Specimens for microstructure and microhardness examination were prepared through the following processes. Firstly, the samples were prepared by cutting 25 ×50 mm cross sections from the welded plates, then the specimens were mounted using a hot mounting press machine and polyfast mounting powder. Grinding and polishing was then carried out on the Struers Labopol 5. This was done in order to maintain an even and clean surface for usage on microscope and micro-hardness tester.

The specimens were then etched using Carpenters reagent [23]. During the etching process, grain boundaries were preferentially attacked, which resulted in a surface characterized by two-dimensional structure that is distinctive when viewed on the microscope. The samples were dipped into the reagent for 10-20 seconds. After the etching process, the samples were then taken to the microscope for observations.

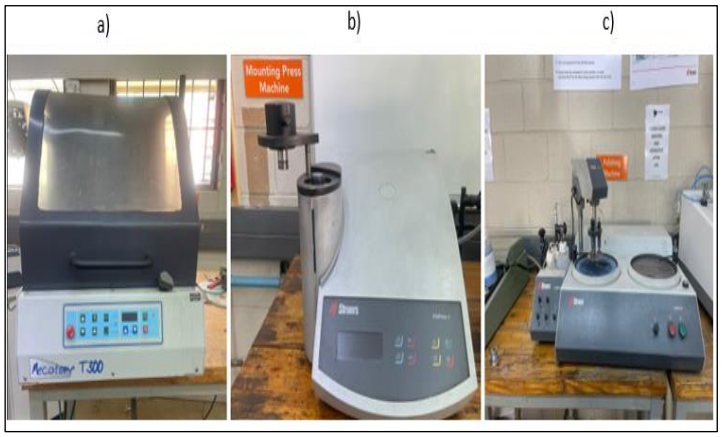

Figure 3: Sample preparation apparatus a) Mecatome T300 cutting machining, b) Hot mounting press machine, and c) Struers Labopol 5 polishing machining.
Source: Authors, (2024).

IV.2 TENSILE TEST

Specimens for tensile testing were machined to size using a Pinnacle PK-GRSM-V milling machine (see Figure 4). The machine specifications are outline in Table 5.

Figure 4: Pinnacle PK-GRSM-V milling machine.
Source: Authors, (2024).

Table 5: Pinnacle PK-GRSM-V milling machine specifications.

Model	PK-GRSM-V
Table size	1270 x 254 mm
Max. Table Load (kgs)	300 kgs
T-Slot (width x number x distance)	16 x 3 x 63.5
Rapid feed rate	890 mm/min

Source: Authors, (2024).

For each HI, three samples were prepared and tested. The tests were carried out in accordance with ASTM E8M-04's specifications as can be seen in Figure 5.

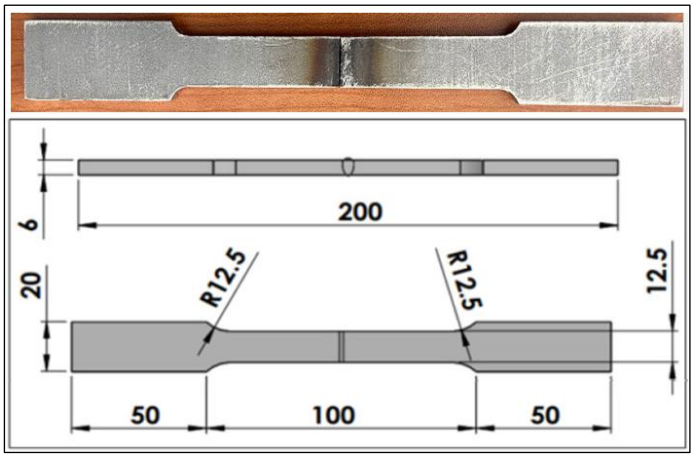

Figure 5: Tensile test specimen (a); dimensions of specimen according to ASTM E8M-04 (b) (units in mm).
Source: Authors, (2024).

V. MEASUREMENT OF OUTPUT PARAMETERS

V.1 MICORSTRUCTURE MEASUREMENT

Metallographic analysis was conducted using Olympus-BX51M optical microscope, shown in Figure 6. The microscope has a magnification range of 5x to 100x.

Figure 6: BX51M Olympus optical microscope.
Source: Authors, (2024).

The system metallurgical microscope has X/Y high speed traveling stage that can position the sample very quickly. The microscope can achieve a resolution of about 100 µm, some of the BX51M Olympus optical microscope's specifications are shown in Table 6.

Table 6: BX51M Olympus optical microscope specifications.

Model	Application	Specifications	
BX51M	Microstructure Chip morphology, and Chip measurements	Resolution	0.37-3.36 µm
		Manual Zooming	5X – 10X
		Working stage	X/Y direction

Source: Authors, (2024).

V.2 MICROHARDNESS MEASUREMENT

Figure 7 shows the Vickers microhardness tester that was used to evaluate the microhardness of the specimens. Depending on the indenter put on the indenter head, this machine can measure both Vickers and Knoop hardness. Eye observation is used to measure the indentation length.

Figure 7: TIME HM-6 digital microhardness tester.
Source: Authors, (2024).

The specifications of the Vickers microhardness testing machine are presented in Table 7. This device features a built-in objective lens with two different magnification settings, 10X and 40X.

Table 7: Micro hardness tester specification.

Model	Application	Specifications	
MH-6	Microhardness	Range	10 - 1000 gf
		Objective	10X and 40X
		Loading rate	60 µm/sec

Source: [24].

The Vickers method is based on an optical measurement system. To create an indentation that can be measured and translated into hardness values, a diamond indenter is used in the microhardness test process described in ASTM C1327-15 [25]. A variety of materials can be processed using this technique. The Vickers scale uses a diamond with a square base and a pyramidal shape (see Figure 8). The load is typically applied for 15 to 30 seconds and ranges from 1 kgf to 120 kgf. Equation 2.1 [26] is used to compute the Vickers number (HV):

$$HV = 1.854 \times \frac{F}{D^2} \quad (2.1)$$

Where:

F = Applied load, kgf
D = Length of the impression diagonal, mm

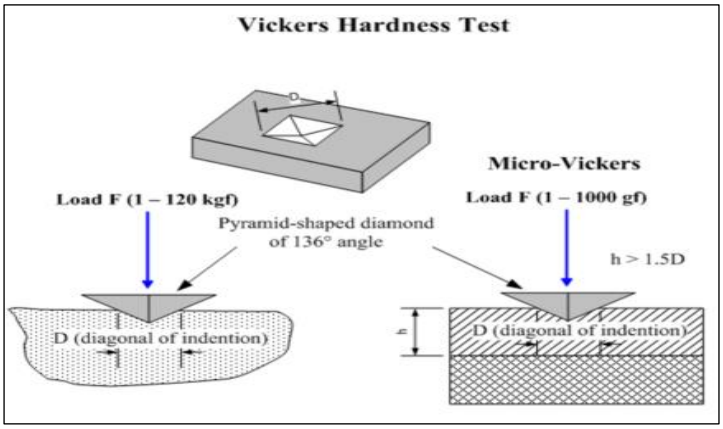

Figure 8: Vickers hardness tester indenter structure.
Source: [24].

A microscope, which is frequently a standard component of the Vickers Tester, is used to measure the length of the impression diagonal. ASTM E-384-99 was followed in conducting the test [27]. The hardness line and track indentation are displayed in Figure 9.

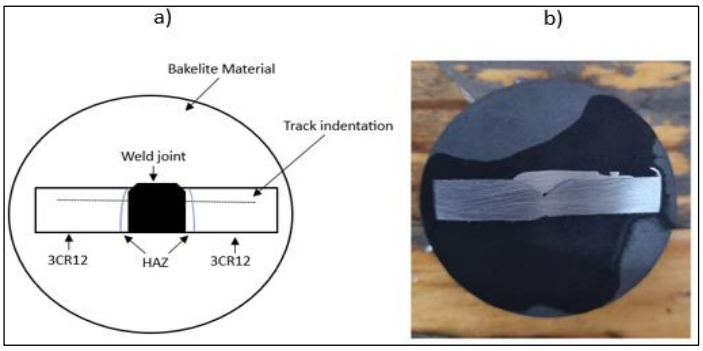

Figure 9: Microhardness test specimens' indentation locations (a) for MIG welded samples (b) after hot mounting.
Source: Authors, (2024).

V.3. TENSILE TESTING

The Instron 9400 tensile testing machine (see Figure 10) was used to conducted tensile testing measurements. This machine is built around an electric motor with variable speed, a gear reduction system, and screws that raise or lower the crosshead. This movement applies tension or compression to the specimen. The motor's speed can be altered to alter crosshead speeds.

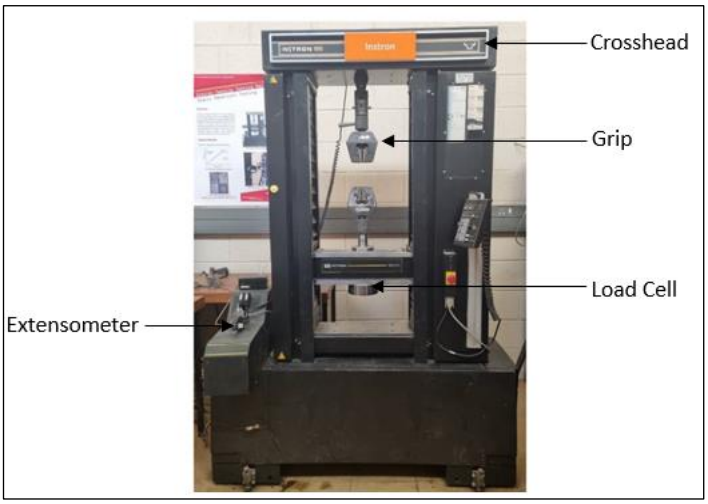

Figure 10: Instron 9400 tensile testing machine.
Source: Authors, (2024).

To successfully test the specimen, the following steps were taken:

1. Put gage marks on the specimen.
2. Measure the initial gage length, width, and thickness.
3. Place the specimen between upper and lower jaw faces.
4. Perform the tensile test.
5. Get the $F - x$ and/or $\sigma - \varepsilon$ data.
6. Measure the final gage length and width.

VI. RESULTS AND DISCUSSIONS

Figure 11 shows a microstructure of a sample that was welded with a HI of 0.35 kJ/mm. The microstructure of the base metal contained ferrite grains with small islands of martensite. Since the 3CR12 stainless steel is Titanium stabilized, the titanium precipitate stabilizers could also be observed in the microstructure of the base metal. The heat-affected zone (HAZ) is characterized by larger coarse grains compared to the base metal, mainly due to the heat applied during the welding process. The grains observed in the microstructure of the HAZ are ferrite grains and small islands of martensite. The ferritic grains observed are dominant in the HAZ, and there is less martensite. Considerable grain growth is observed at the HAZ closer to the weld zone, and the grain size decreases when observed further away from the weld zone.

The microstructure observed in the weld zone mainly consists of fine grains of austenite and small portions of ferrite. The observed austenitic microstructure is due to the filler metal used in the welding process, which is 308L, an austenitic stainless steel grade, and the different phases present in the weld zone are due to welding a ferritic steel base metal using an austenitic grade filler metal.

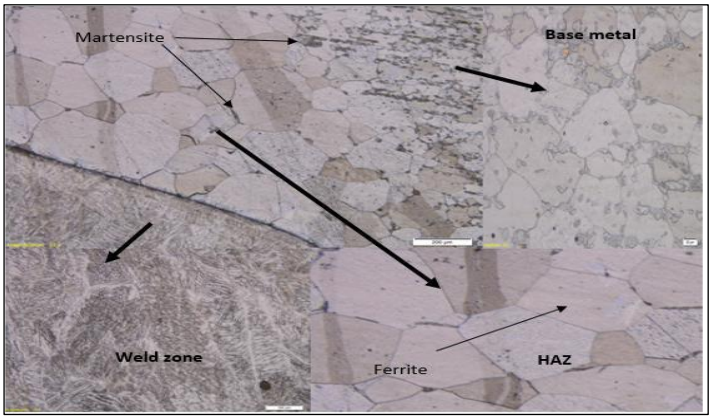

Figure 11: Sample welded at a heat input of 0.35 kJ/mm.
Source: Authors, (2024).

Figure 12 shows a microstructure of a sample that was welded with a HI of 0.35 kJ/mm. The microstructure of the base metal contained ferrite grains with small islands of martensite, like the first sample. This is attributed to the fact that the increase in HI is insignificant (0.05kJ/mm) hence the similarities.

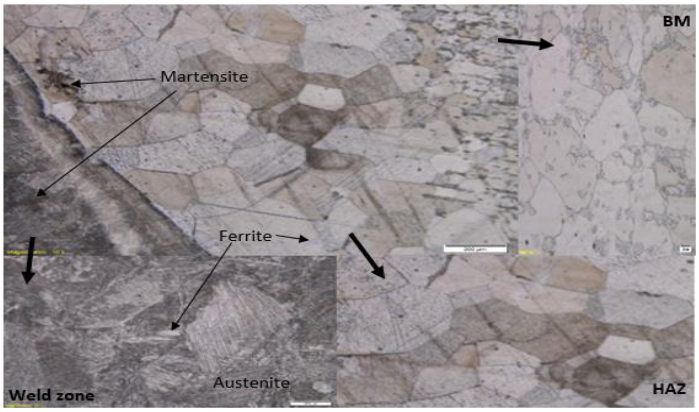

Figure 12: Sample welded at a heat input of 0.45 kJ/mm.
Source: Authors, (2024).

Figure 13 shows a microstructure of the weldment using a HI of 1.0kJ/mm. the microstructure exhibited an acicular ferrite and lathe martensite. The lath martensite was widely dispersed. The presence of martensite was observed to be higher toward the center of the weld. This is mainly due to the high heat application and the higher rate of cooling at the center of the weld than in the zones toward the fusion zone.

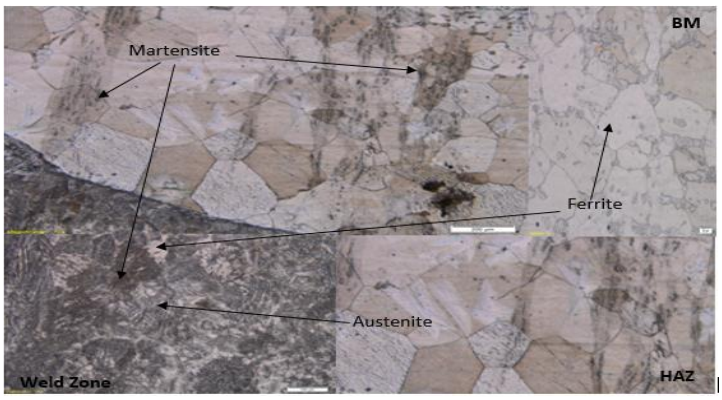

Figure 13: Sample welded at a heat input of 1.0 kJ/mm.
Source: Authors, (2024).

Figure 14, and 15 shows the microstructures of the weldment using a HI of 1.65, and 1.75kJ/mm respectively. Both these HI are then the optimal recommended range of welding 3CR12. The microstructure also exhibited a lath martensite with a higher amount of martensite with a higher amount of martensite.

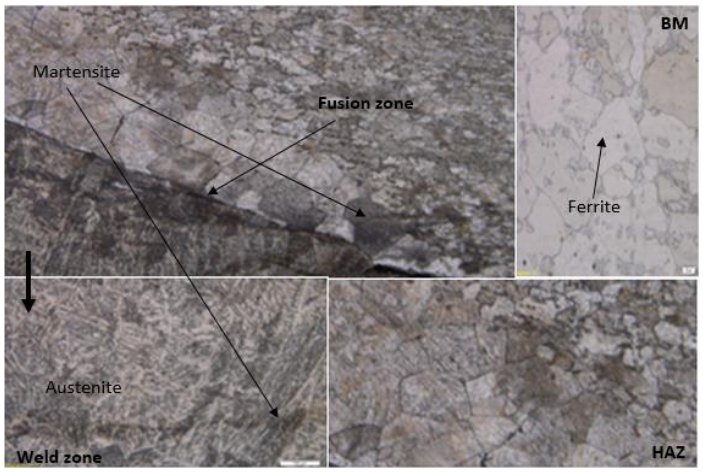

Figure 14: Sample welded at a heat input of 1.65 kJ/mm.
Source: Authors, (2024).

Excessive grain deformation can be observed in the HAZ of sample 4. The HAZ is characterized by larger coarse grains similar to the other samples discussed. However, the grain boundaries of the observed grains are not as defined as those of sample 1 to sample 3. Martensite laths can be observed in the HAZ microstructure. The martensite presence observed is significantly more than in the first three samples due to the excessive heat input used to weld the sample. Considerable grain growth is observed at the HAZ closer to the weld zone, and the grain size decreases when observed further away from the weld zone.

The microstructure observed in the weld zone consists of fine grains of austenite and ferrite with martensite laths. The ferrite content in the weld zone is significantly less than in the first three samples. The martensite laths observed are at different orientations across the microstructure of the weld zone, and the presence of the martensite laths is more than in the first three samples as the heat input is also significantly higher than in the first three samples.

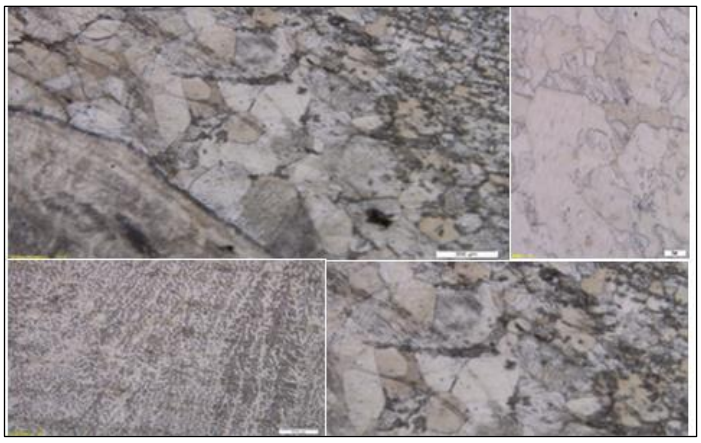

Figure 15: Sample welded at a heat input of 1.75 kJ/mm.
Source: Authors, (2024).

Excessive grain deformation can be observed in the HAZ of sample 5, similar to the microstructure observed in sample 4. However, the grain deformation is more in sample 5 than in sample 4. The HAZ is characterized by larger coarse grains similar to all the samples discussed. However, the grain boundaries of the observed grains are not as defined as those of sample 1 to sample 3 and are defined similarly to those observed in sample 4. Martensite can be observed in the HAZ microstructure. The martensite presence observed is significantly more than all the other samples due to the excessive heat input welding the sample, which is 1.75kJ/mm. Considerable grain growth is observed at the HAZ closer to the weld zone, and the grain size decreases when observed further away from the weld zone. The microstructure observed in the weld zone consists of fine grains of austenite and ferrite with martensite laths. The ferrite content in the weld zone is significantly less than all the other samples. The martensite laths observed are at different orientations across the weld microstructure.

VI.1 MICROSTRUCTURE SUMMARY

The base metal's microstructure, 3CR12 stainless steel, was observed to have a dual phase of ferrite and martensite. This is consistent with the microstructure observed by Akinlabi and Akinlabi when characterizing the effect of heat treatment on 3CR12 stainless steel [28]. The ferrite grains were observed to be the white phase, whereas the martensite phase was the dark phase. This dual-phase presence in the base metal of 3CR12 stainless steel elucidates the fluctuations observed in the microhardness profile in the base metal. The higher values were due to the indentation occurring where martensite was present, and the lower values were due to the indentation occurring on the ferrite grains.

The microstructure in the weld zone of the welded sample was observed to have three phases: austenite, ferrite, and martensite. This mixture of phases is due to welding 3CR12 stainless steel, a ferritic steel base metal using an austenitic grade filler metal of 308L. The 308L was recommended to be the optimum filler material for welding 3CR12 stainless steel from the work of Molabe [29], and the observed microstructure is consistent with that observed from the same work. And hence the austenitic microstructure is due to the use of the 308L filler material grade. Martensite laths could be observed at different orientations in all the welded specimens, and higher heat inputs yielded more martensite presence. This elucidates the hardness values recorded in the weld zone, which were more than those observed in the HAZ and the base metal. An increase in the hardness values in the weld zone was influenced by the increase in the heat input and, thus, the presence of martensite.

VI.2 GRAIN SIZE CHARACTERIZATION

A solid metal's grain is made up of a variety of small crystals that are dispersed at random. Most mechanical qualities, such as hardness, yield strength, tensile strength, and impact strength, can be measured in relation to grain size. All these mechanical properties aforementioned increase with a decrease in grain size. Quantifying and characterizing the observed grain deformation that has happened in the changing microstructures of the welded material. The size of each grain in the microstructures was measured using the measuring instrument on the optical microscope.

During the microstructural analysis of the samples welded at various heat inputs, an alteration in the size of the grains in the heat-affected zone was observed. The areas of the 3CR12 stainless steel susceptible to heat application during the welding process showed a significant increase in grain size. The grain size affects the properties of a material, such as hardness. The grains that could

be correctly observed in the different samples were measured using the optical microscope and presented in Figures 16 to 20.

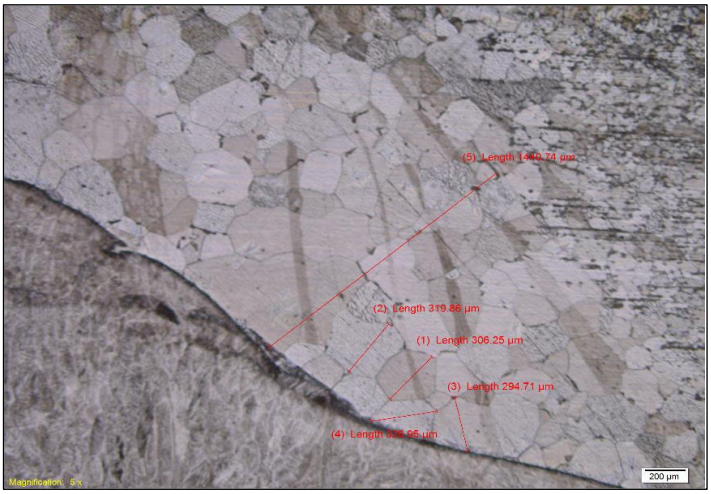

Figure 16: Sample welded at a heat input of 0.35 kJ/mm.
Source: Authors, (2024).

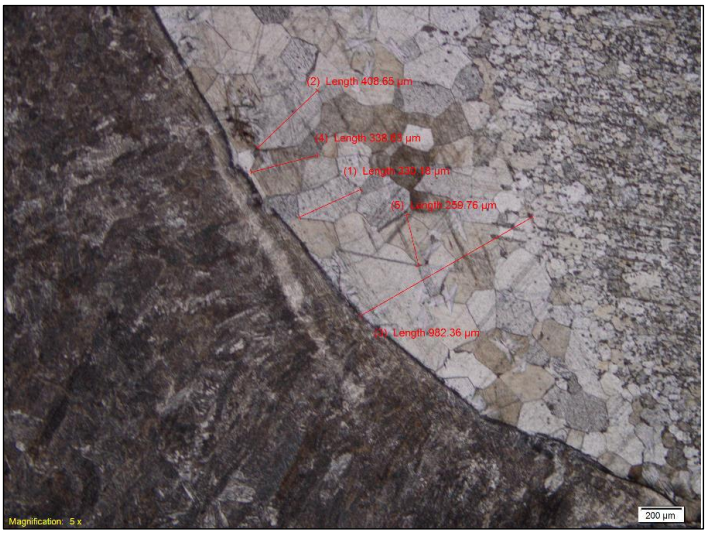

Figure 17: Sample welded at a heat input of 0.45 kJ/mm.
Source: Authors, (2024).

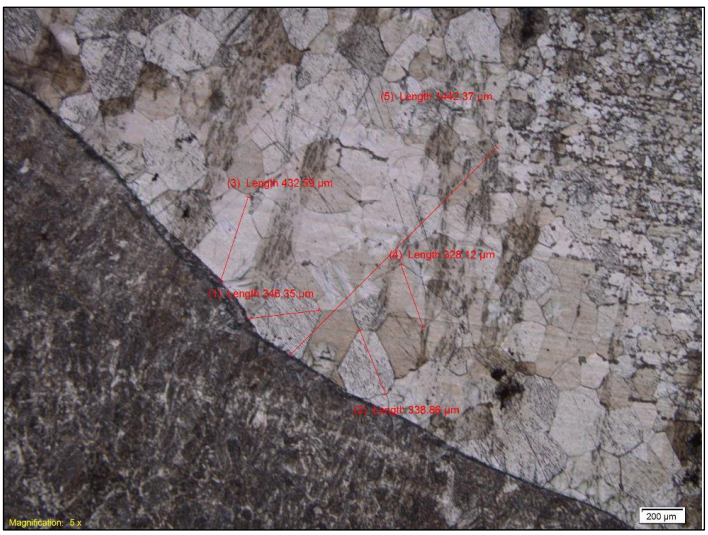

Figure 18: Sample welded at a heat input of 1.0 kJ/mm.
Source: Authors, (2024).

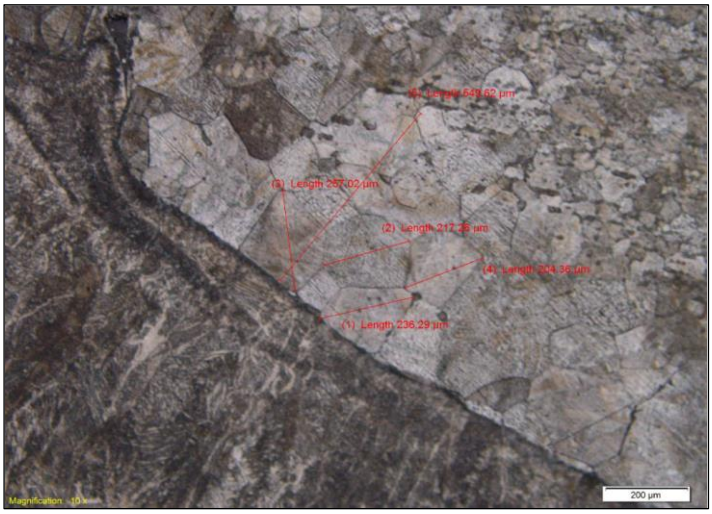

Figure 19: Sample welded at a heat input of 1.65 kJ/mm.
Source: Authors, (2024).

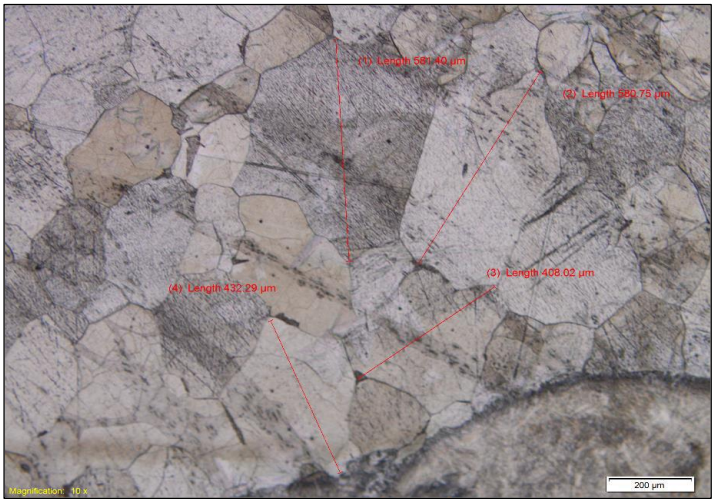

Figure 20: Sample welded at a heat input of 1.75 kJ/mm.
Source: Authors, (2024).

VI.2.1 Grain Size Characterization Summary

The grain sizes are summarized in Table 8, where the measurements of 4 grains per sample and an average value are determined.

Table 8: Summary of the grain sizes for each sample.

Measurement	Grain size (µm)				
	0.35kJ/mm	0.45kJ/mm	1.0kJ/mm	1.65kJ/mm	1.75kJ/mm
1	326.95	408.65	432.59	236.29	290.7
2	319.86	338.63	346.35	204.36	290.38
3	306.25	330.13	328.12	257.02	216.15
4	294.71	253.76	338.86	217.26	204.01
Average	311.9	332.79	361.48	228.73	250.31

Source: Authors, (2024).

An interesting observation was seen that an increase in the HI resulted in an increase in the grain size, only up to a certain extent. (HI, 0.35-1.0kJ/mm). Future increase resulted in a reduction in grain size. The microstructure of the HAZ for all the welded samples is characterized by enlarged and coarse grains in all the welded samples due to the application of heat during welding. Similar results were observed [28], [30]. The increase in the grain

size implies that fewer grain boundaries are present in the HAZ of the weld, and according to Vithi et al. [31] the presence of fewer grains in the microstructure makes the HAZ susceptible to dislocation movement. Dislocation movement results in a decrease in strength and thus makes the HAZ defenseless against fracture. An increase in the grain size resulted from the increase in the heat input. This also increased the volume of martensite precipitate present in the HAZ. The microstructure of the HAZ is characterized by the dual phases consisting of ferrite and martensite as with the base metal. This also elucidates the fluctuations observed in the microstructure of the HAZ is characterized by the dual phases consisting of ferrite and martensite as with the base metal. This also elucidates the fluctuations observed in the microhardness profile of the hardness in HAZ for all the welded samples. The higher values were due to the indentation occurring where martensite was present, and the lower values were due to the indentation occurring on the ferrite grains as with the base metal. An increase in grain size reduces the ductility and, thus, the material's toughness. However, according to Molabe [29], the grain growth was determined to have little to no effect on the tensile strength of 3CR12 stainless steel. This was due to the fracture during tensile testing occurring at the base metal instead of the HAZ. This is also consistent with the results obtained by Vithi et al. [31], where the fracture during tensile testing occurred in the base metal.

VI.3 MICROHARDNESS

The Vickers microhardness of the different samples was measured from the center of the weld to the base metal, and the profile obtained from the microhardness values for the different samples is shown in Figure 21. The different welded samples have the same base material, 3CR12 stainless steel. A fluctuation in the hardness profile can be observed in the base metal. This is mainly due to the alternating phases of ferrite and martensite found in the microstructure of the base metal. The martensite portions produce higher hardness values, whereas the ferrite grains produce lower hardness values, resulting in fluctuating values. However, the average hardness value found at the base metal is 178HV. The hardness values observed at the fusion zone (FZ), or weld cap are higher than the hardness values of both the base metal and the HAZ, with the lowest hardness observed at the HAZ. This phenomenon was observed for all the welded samples.

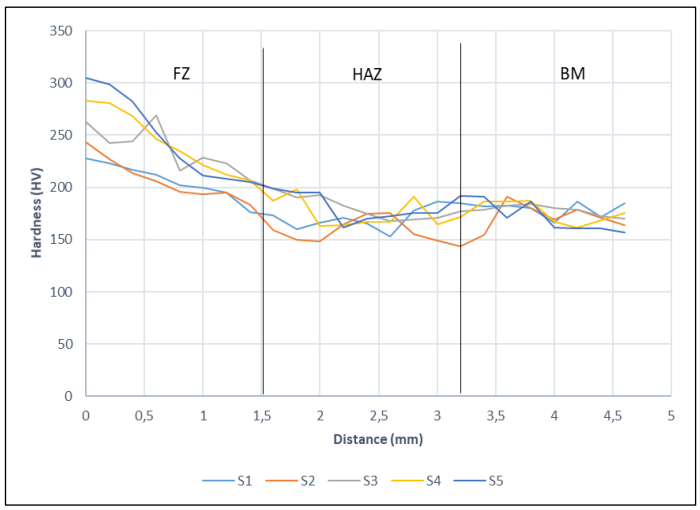

Figure 21: Vickers microhardness profiles of the samples.
Source: Authors, (2024).

VI.4 TENSILE TESTING

According to the results of the tensile testing, all of the weldments have fractures in the weld zone (WZ) region (see Figure 22). This indicates that the WZ area, which has low tensile strength, is the weakest component of the joint. The site of the fracture was connected to the welding-induced decrease in the weld's hardness and strength. Precipitate coarsening in the over-aged zone was the main reason for the dramatic decrease in strength.

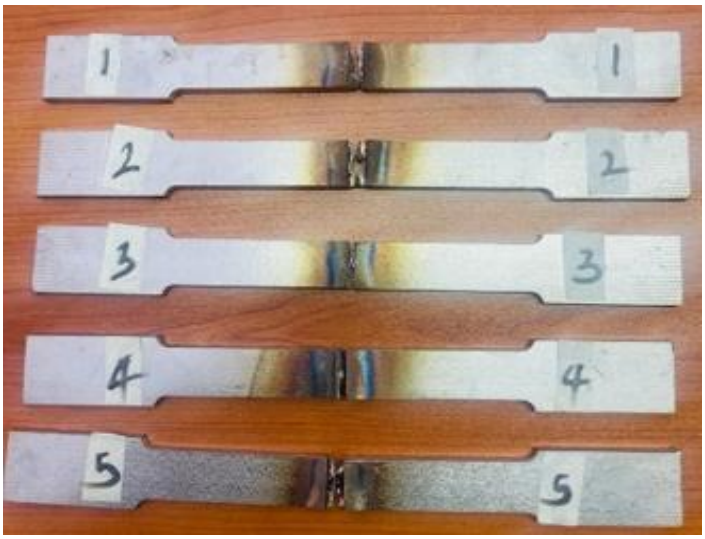

Figure 22: Fracture location of tensile testy samples.
Source: Authors, (2024).

Analyzing the results presented in Table 9, it can be argued that by changing the HI, it is possible to ensure the required strength of the welded joint. Controlled heat input welding procedures within the acceptable standard [18], [19], [22] ensures excellent strength of the welded joints.

The tensile tests of the welded specimens revealed a striking decrease in tensile strength when compared to values of the base material. About 45% of the base metal strength was the tensile strength of the weld joint.

Table 9: Summary of tensile test results.

HI (kJ/mm)	Load (N)	Average Load (N)
0.35	17349.85	16166.56
	15561.68	
	15588.16	
0.45	13355.09	17174.48
	21342.77	
	16825.57	
1.0	17989.06	20865.95
	21023.35	
	23585.45	
1.65	16838.97	22362.94
	23593.52	
	26656.34	
1.75	27431.8	24705.47
	20799.42	
	25885.2	

Source: Authors, (2024).

VII. CONCLUSIONS

Investigations were made into the ferritic stainless steel 3CR12's microstructure and mechanical characteristics. The study led to the following crucial conclusions. The coarse ferrite grains in the base metal are changed to fine grains of ferrite with some grain boundary lath martensite as a result of characteristic rapid solidification. The hardness at the mid cross-section of the fusion zone was found to be higher than the base material. This is mainly due to the fine solidification structure as a result of fast solidification.

VIII. AUTHOR'S CONTRIBUTION

Conceptualization: Thabo Nelson Mathonsi.
Methodology: Thabo Nelson Mathonsi
Investigation: Thabo Nelson Mathonsi
Discussion of results: Thabo Nelson Mathonsi
Writing – Original Draft: Thabo Nelson Mathonsi.
Writing – Review and Editing: Thabo Nelson Mathonsi
Approval of the final text: Thabo Nelson Mathonsi

IX. REFERENCES

[1] V. Balasubramanian, A. Lakshminarayanan, R. Varahamoorthy and S. Babu, "Application of Response Surface Methodology to Prediction of Dilution in Plasma Transferred Arc Hardfacing of Stainless Steel on Carbon Steel," International Journal of Iron Steel Res, vol. 16, pp. 44-53, 2009.

[2] AWS, "Welding Handbook: Welding Processes," in American Welding Society, vol. 2, 1992, p. 955.

[3] S. Brandi, S. Lui and T. Junior, "Welding, Brazing and Soldering, Electroslag and Electrogas Welding. ASM Handbook," ASM International, vol. 15, pp. 124-38, 2008.

[4] M. Butt, M. Ahmad and M. Azha, "Characterization for GTAWAISI 316 to AISI 316 & SA 516 Grade 70 Steels with Welded & Prewelded Annealing Conditions," Journal of Quality Technology Management , vol. 8, no. 2, pp. 119-33, 2012.

[5] N. G. Jungbacke, "The Influence of Substitutional Elements on the Transformability of 3CR12 Steel," University of Cape Town, Cape Town, 1996.

[6] A. K. Lakshminarayanan and V. Balasubramanian, "Evaluation of Microstructure and Mechanical Properties of Laser Beam Welded AISI 409M Grade Ferritic Stainless Steel," International Journal of Iron and Steel Research, vol. 19, no. 1, pp. 72-77, 2012.

[7] R. D. Knutsen, "A Microstructural Examination of Duplex Ferrite-martensite Corrosion Resisting Steels," University of Cape Town, Cape Town, 1989.

[8] J. Tarboton, " Johannes Paulus Hoffman The Technical Father of 3CR12," South African Institute of Mining and Metallurgy, vol. 116, no. 8, pp. 6-7, 2016.

[9] M. Greef, "The Influence of Welding Parameters of the Senitisation behaviour of 3CR12," University of Pretoria, Pretoria, 2006.

[10] "Stainless Steel," Columbus Stainless Pty Ltd, [Online]. Available: https://www.columbus.co.za/. [Accessed 10 July 2023].

[11] B. Rossi, "Mechanical Properties, Residual Rtresses and Structural behavior of Thin-walled Stainless Steel Profiles. PhD Thesis," University of Liège, Liège, 2008.

[12] A. Kaymakci, D. M. Madyira and N. Nkwanyana, "The Effect of Metal Transfer Modes on Mechanical Properties of 3CR12 Stainless Steel," Trascations of the Canadian Society for Mechanial Engineering, vol. 44, no. 2, 2019.

[13] S. S. R. Singh, R. V. Praneeth, V. S. Sankalp, S. S. Sashank and R. Karthikeyan, "Welding, Mechanical Properties and Microstructure of Different Grades of Austenitic Stainless Steels: A Review," Materials Today: Proceedings, vol. 62, pp. 3675-3680, 2022.

[14] F. S. d. Luz, W. A. Pinheiro, S. N. Monteiro, V. S. Candido and A. C. R. d. Silva, "Mechanical Properties and Microstructural Characterization of A Novel 316L Austenitic Stainless Steel Coating on A516 Grade 70 Carbon Steel Weld," Journal of Materilas Research and Technology, vol. 9, no. 1, pp. 636-640, 2020.

[15] S. Wu, T. Xu, M. Song and K. Guan, "Mechanical Properties Characterization of Welded Joint of Austenitic Stainless Steel using Instrumented Indentation Technique," Materials at High Temperature, vol. 33, no. 3, 2016.

[16] R. Krawczyk, J. Słania, G. Golański and T. Pfeifer, "Mechanical Properties and Microstructure of Austenite - Ferrite Duplex Stainless Steel Hybrid (Laser + GMAW) and SAW Welded Joint," Materials Basel, vol. 16, no. 7, 2023.

[17] R. M. C. Molabe, "Determining the Optimum Welding Material of 3CR12 Stainless Steel - Master Dessertation," Department of Mechanical Engineering - University Of Johannesburg, Johannesburg, 2018.

[18] J. Luijan, P. Surin and K. Eidhed, "The Effect of Welding Parameters on Joining Dissimilar Low Carbon Steel and 3CR12 Ferritic Stainless Steel by GTAW with ER308L Filler Metal," Journal of Physics: Conference Series, vol. 1519, 2020.

[19] K. Touileb, A. C. Hedhibi, R. Djoudjou, A. Ouis, A. Bensalama, A. Ibrahim, H. S. Abdo and M. M. Z. Ahmed, "Mechanical, Microstructure, and Corrosion Characterization of Dissimilar Austenitic 316L and Duplex 2205 Stainless-Steel ATIG Welded Joints," Materials (Basel), vol. 15, no. 7, p. 2470, 2022.

[20] "Stainless Steel 3CR12 Technical Data," Macsteel, [Online]. Available: https://macsteel.co.za/wp-content/uploads/2022/12/3CR12-data-sheet-2021.pdf. [Accessed 10 July 2023].

[21] "AR Series AR 1440 - Technical Details," Yaskawa, 2023. [Online]. Available: https://www.yaskawa.za.com/products/robots/welding-cutting/productdetail/product/ar1440_734. [Accessed 10 July 2023].

[22] K. Mogano, "Effect of Multipass Welding on Mechanical Properties of 3CR12 Steel - Masters Dessertation," Department of Mechanical Engineering University of Johannesburg, Johannesburg, 2021.

[23] K. B. Small, D. A. Englehart and T. A. Christman, "Technical Guide - A Guide to Etching Specialty Alloys for Microstructural Evaluation," Carpenter Technology, 2023. [Online]. Available: https://www.carpentertechnology.com/blog/a-guide-to-etching-specialty-alloys. [Accessed 11 July 2023].

[24] "Hardness Test Methods," SubsTech, 03 May 2014. [Online]. Available: https://www.substech.com/dokuwiki/doku.php?id=hardness_test_methods. [Accessed 15 April 2022].

[25] "Standard Test Method for Vickers Indentation Hardness of Advanced Ceramics," ASTM International C1327-15 (2019), 09 July 2019. [Online]. Available: https://compass.astm.org/document/?contentCode=ASTM%7CC1327-15R19%7Cen-US. [Accessed 15 March 2022].

[26] R. Smallman and A. Ngan, Modern Physical Metallurgy, Elsevier Ltd, 2014.

[27] "ASTM International - ASTM E384-99: Standard Test Method for Microindentation Hardness of Materials," ASTM International, 2023. [Online]. Available: https://standards.globalspec.com/std/3805697/ASTM%20E384-99. [Accessed 10 July 2023].

[28] E. T. Akinlabi and S. A. Akinlabi, "Characterising the Effects of Heat Treatment on 3CR12 and AISI 316 Stainless Steels," International Journal of Mechanical, Aerospace, Industrial and Mechatronics Engineering, vol. 8, no. 2, 2014.

[29] M. R. C. Molabe, "Determining the Optimum Welding Material of 3CR12 Stainless Steel," Department of Mechanical Engineering - University of Johnnesburg, University of Johnnesburg, 2018.

[30] C. C. Silva, J. P. Farias, H. C. Miranda, R. F. Guimarães, J. W. A. Menezes and M. A. M. Neto, "Microstructural characterization of the HAZ in AISI 444 Ferritic Stainless Steel Welds," Material Characterization, vol. 59, no. 5, pp. 528-528, 2008.

[31] N. L. Vithi, M. G. Maruma, A. Maleka and D. Chetty, "Microstructural and Mechanical Properties of Joining 3CR12 Stainless Steel and S355 Carbon Steel by GMAW Using 308L Filler Wire," Composite Materials, vol. 6, no. 1, pp. 1-6, 2022.